

Proposal for an Electron Antineutrino Disappearance Search Using High-Rate ${}^8\text{Li}$ Production and Decay

A. Bungau¹, A. Adelmann², J.R. Alonso³, W. Barletta³, R. Barlow¹, L. Bartoszek⁴, L. Calabretta⁵, A. Calanna³, D. Campo³, J.M. Conrad³, Z. Djurcic⁶, Y. Kamyshkov⁷, M.H. Shaevitz⁸, I. Shimizu⁹, T. Smidt³, J. Spitz³, M. Wascko¹⁰, L.A. Winslow³, J.J. Yang^{2,3}

¹ University of Huddersfield, Huddersfield, HD1 3DH, UK

² Paul Scherrer Institut, Villigen, CH-5232, Switzerland

³ Massachusetts Institute of Technology, Cambridge, MA 02139, USA

⁴ Bartoszek Engineering, Aurora, IL 60506, USA

⁵ Istituto Nazionale di Fisica Nucleare, Laboratori Nazionali del Sud, I-95123, Italy

⁶ Argonne National Laboratory, Argonne, IL 60439, USA

⁷ University of Tennessee, Knoxville, TN 37996, USA

⁸ Columbia University, New York, NY 10027, USA

⁹ Tohoku University, Sendai, 980-8578, Japan and

¹⁰ Imperial College London, London, SW7 2AZ, United Kingdom

This paper introduces an experimental probe of the sterile neutrino with a novel, high-intensity source of electron antineutrinos from the production and subsequent decay of ${}^8\text{Li}$. When paired with an existing ~ 1 kton scintillator-based detector, this $\langle E_\nu \rangle = 6.4$ MeV source opens a wide range of possible searches for beyond standard model physics via studies of the inverse beta decay interaction $\bar{\nu}_e + p \rightarrow e^+ + n$. In particular, the experimental design described here has unprecedented sensitivity to $\bar{\nu}_e$ disappearance at $\Delta m^2 \sim 1 \text{ eV}^2$ and features the ability to distinguish between the existence of zero, one, and two sterile neutrinos.

PACS numbers: 14.60.Pq, 14.60.St

The beta decay-at-rest of ${}^8\text{Li}$ produces an isotropic electron antineutrino flux with an average energy of 6.4 MeV. An underground liquid scintillator based detector can be used to detect these antineutrinos via the inverse beta decay (IBD) process $\bar{\nu}_e + p \rightarrow e^+ + n$. The antineutrino rate and energy, peaking at 9 MeV, can be fully reconstructed by the detector. Precise energy and vertex reconstruction opens the possibility of searching for antineutrino disappearance due to oscillations, which, in the simplest two-neutrino form, has the probability

$$P = 1 - \sin^2 2\theta \sin^2 [1.27 \Delta m^2 (L/E)], \quad (1)$$

where θ is the disappearance mixing angle; Δm^2 (eV 2) is the squared mass splitting; L is the distance (in meters) from the antineutrino source to the detector; and E (MeV) is the antineutrino energy. This probability is maximized in the range of $\Delta m^2 \sim E/L$. An existing large scintillator-based antineutrino detector with a diameter of $\mathcal{O}(10 \text{ m})$, when combined with an ${}^8\text{Li}$ isotope decay-at-rest source, is sensitive to oscillations at $\Delta m^2 \sim 1 \text{ eV}^2$. This is an oscillation region of high interest due to anomalies that have been observed in the data from LSND [1], MiniBooNE [2], short-baseline reactor studies [3], and gallium source calibration runs [4]. These anomalies are often interpreted as being due to sterile neutrinos [5–8] and have motivated the development of the IsoDAR (Isotope Decay-At-Rest) concept.

IsoDAR-style sources have been considered before [9–11]. The design presented here, consisting of an ion source, cyclotron, and target, is the first with a sufficiently high antineutrino flux to address the existence of one or more sterile neutrinos. The ${}^9\text{Be}$ target, used

mainly as an intense source of beam-induced neutrons, is surrounded by a ${}^7\text{Li}$ sleeve. When the target and sleeve combination is placed next to a kiloton-scale scintillator detector (e.g., KamLAND [12], SNO+ [13], or Borexino [14]), the large antineutrino flux from ${}^8\text{Li}$ beta decay can result in the collection of over 8×10^5 IBD interactions in a five year run. Such events allow a definitive search for antineutrino oscillations with the added ability to distinguish between models with one and two sterile neutrinos. A sample of more than 7200 $\bar{\nu}_e$ -electron scatters is also accumulated during this time and can be used as a sensitive electroweak probe.

The charged particle beam, used for electron antineutrino production, originates with a 60 MeV/amu cyclotron accelerating 5 mA of H_2^+ ions. The design of this compact cyclotron [15] is ongoing and is envisaged as the injector for the accelerator system of the DAE δ ALUS physics program [16, 17]. The IsoDAR design calls for about a factor of six increase in intensity compared to compact cyclotrons used in the medical isotope industry. Current and future medical isotope machines accelerate protons to 60 MeV and beyond with average intensities of 0.8 – 1.6 mA [18, 19].

In our design, a 5 mA H_2^+ beam is injected at 70 keV (35 keV/amu) via a spiral inflector. Existing ion sources are sufficient to supply the beam required [20]. In the low-energy regime, space charge is crucial in modeling the beam dynamics correctly. The generalized permeance of a non-neutral beam, $K = qI/(2\pi\epsilon_0 m\beta^3\gamma^3)$, parameterizes the strength of the space charge effect [21]. We conclude that the K for this machine is of the same order as existing proton machine designs based on ≈ 2 mA and

an injection energy of 30 keV [22, 23]. The proposed high power is therefore feasible with regard to space charge issues.

The accelerator described is a continuous-wave source with a 90% duty cycle to allow for machine maintenance. In consideration of target cooling and degradation with 600 kW of beam power, we require a uniform beam distributed across most of the 20 cm diameter target with a sharp cutoff at the edges. Third-order focussing elements in the extraction beam line are able to convert the Gaussian-like beam distribution into a nearly uniform one [24] and hence create the necessary condition on the target.

The 60 MeV proton beam impinges on a cylindrical ^{9}Be target that is 20 cm in diameter and 20 cm long. The primary purpose of this target is to provide a copious source of neutrons. Neutrons exiting the target are moderated and multiplied by a surrounding 5 cm thick region of D_2O , which also provides target cooling. Secondary neutrons enter a 150 cm long, 200 cm outer diameter cylindrical sleeve of solid lithium enveloping the target and D_2O layer. The target is embedded 40 cm into the upstream face of this volume; a window allows the beam to reach the target. The sleeve is composed of isotopically enriched lithium, 99.99% ^{7}Li compared to the natural abundance of 92.4%. The isotopically pure material is widely used in the nuclear industry and is available from a number of sources. The isotope ^{8}Li is formed by thermal neutron capture on ^{7}Li and to a lesser extent by primary proton interactions in the ^{9}Be target. For enhanced production, the sleeve is surrounded by a volume of graphite and steel acting as a neutron reflector and shield. The volume extends 2.9 m in the direction of the detector. Isotope creation in the shielding is negligible. Figure 1 displays the target and sleeve geometry, and Table I summarizes the experimental parameters. We note that the geometry of the design is similar to that described in Ref. [10].

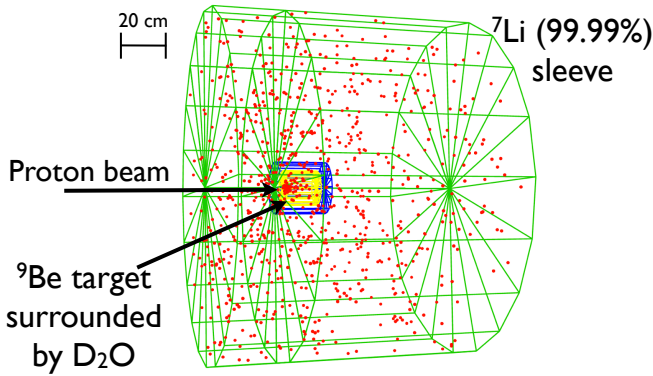


FIG. 1: A schematic of the IsoDAR target and surrounding volumes. The dots represent ^{8}Li ($\bar{\nu}_e$) creation points, obtained with 10^5 60 MeV protons on target simulated. The neutron reflector, shielding, and detector are not shown.

Accelerator	60 MeV/amu of H_2^+
Current	10 mA of protons on target
Power	600 kW
Duty cycle	90%
Run period	5 years (4.5 years live time)
Target	^{9}Be surrounded by ^{7}Li (99.99%)
$\bar{\nu}$ source	^{8}Li β decay ($\langle E_{\nu} \rangle = 6.4$ MeV)
$\bar{\nu}_e/1000$ protons	14.6
$\bar{\nu}_e$ flux	$1.29 \times 10^{23} \bar{\nu}_e$
Detector	KamLAND
Fiducial mass	897 tons
Target face to detector center	16 m
Detection efficiency	92%
Vertex resolution	$12 \text{ cm}/\sqrt{E} \text{ (MeV)}$
Energy resolution	$6.4\%/\sqrt{E} \text{ (MeV)}$
Prompt energy threshold	3 MeV
IBD event total	8.2×10^5
$\bar{\nu}_e$ -electron event total	7200

TABLE I: The relevant experimental parameters used in this study.

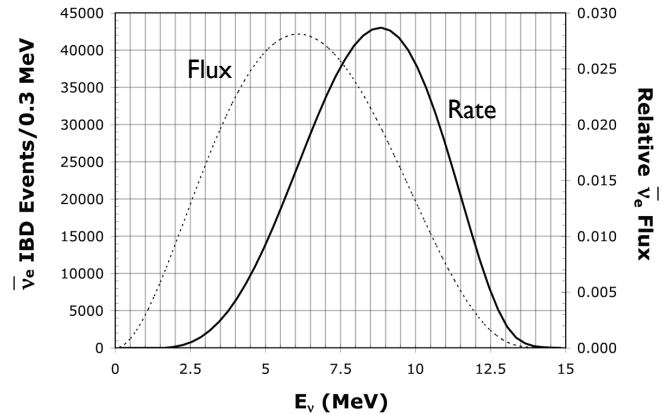


FIG. 2: The expected antineutrino flux and detected event rate in the experimental configuration considered. The antineutrino flux mean energy from ^{8}Li is 6.4 MeV. There are 8.2×10^5 reconstructed events expected from the $1.29 \times 10^{23} \bar{\nu}_e$ created in the target and sleeve in five years.

We determine isotope production rates using a GEANT4 simulation [25]. Due to its vast range of applications, GEANT4 provides an extensive set of data-based, parametrized, and theory-driven hadronic models, each one specializing in different types of interactions within a specified range of energy. The QGSP-BIC-HP physics package was chosen for this particular application. The applicable physics model is the pre-compound nuclear one which is invoked by the Binary Cascade simulation. Simulated hadronic processes include elastic scattering, inelastic scattering, neutron capture, neutron fission, lepton-nuclear interactions, capture-at-rest, and charge exchange. For neutron energies below 20 MeV, the high-precision package uses the ENDF/B-VII data library [26].

Although all isotopes are considered in this analysis,

the induced ${}^8\text{Li}$ source in the sleeve dominates the antineutrino flux. The simulation yields 14.6 ${}^8\text{Li}$ isotopes for every 1000 protons (60 MeV) on target. Approximately 10% of all ${}^8\text{Li}$ is produced inside the target; the rest is produced in the sleeve. Neutrinos and antineutrinos from other unstable isotopes are produced at a comparatively negligible rate. Over a five year run period and with a 90% duty cycle, 1.29×10^{23} antineutrinos from ${}^8\text{Li}$ are created. IsoDAR's nominal oscillation analysis is done in terms of "shape-only" in L/E and is therefore independent of the absolute flux normalization. However, a "rate+shape" analysis using an absolute flux normalization uncertainty of 5% is also considered in this study.

The IsoDAR antineutrino source is paired with an existing underground scintillator-based detector for characterizing the antineutrino flux as a function of distance and energy. As can be seen in Eq. 1, a baseline of $L \sim 10$ m is appropriate as a probe of the $\Delta m^2 \sim 1$ eV 2 region given the antineutrino spectrum shown in Fig. 2. We assume the face of the target sits 16 m from the center of a KamLAND-inspired 897 ton detector when calculating rates and oscillation sensitivity.

The $\bar{\nu}_e$ events are detected through the IBD interaction, which is unique in several ways. IBD has a comparatively high cross section ($\sim 3 \times 10^{-42}$ cm 2) which is known to < 1% across the relevant energy range [27]. The distinct delayed coincidence signal of prompt light from the positron, followed by a 2.2 MeV gamma from the neutron capture on a proton, enables a low background rate expectation. The antineutrino energy can be fully reconstructed on an event-by-event basis using the visible energy of the prompt positron signal in the detector: $E_{\bar{\nu}_e} = E_{e^+} + 0.78$ MeV. A prompt energy threshold of 3 MeV is employed here. In a five year run, 8.2×10^5 reconstructed signal events are expected with 92% detection efficiency [28] and in the absence of antineutrino oscillations.

The unique delayed coincidence signal makes reactor antineutrinos the only significant background in this analysis. The reactor antineutrino event rate at KamLAND is on the order of 100 events per year [29], uniformly distributed across the detector. At SNO+, the reactor background would be a factor of about five lower [30]. There is 9.4 m of passive and active shielding in between the end of the sleeve and the beginning of the fiducial volume, including an instrumented water veto detector. This shielding is adequate for attenuating/eliminating beam-related neutrons that can produce an IBD-like background, especially in consideration of the 3 MeV prompt energy threshold requirement. Furthermore, the sinusoidal-wave-like nature of an expected oscillation signal in L/E cannot be mimicked by background.

To perform an oscillation analysis, the antineutrino travel distance (L) and energy (E) must be reconstructed simultaneously on an event-by-event basis. Using KamLAND's detection capability as an exam-

ple for the performance of a large scintillator detector, the energy can be reconstructed with a resolution of $6.4\%/\sqrt{E}$ (MeV) [28]. With the antineutrino event vertex in the detector known to within $12\text{ cm}/\sqrt{E}$ (MeV) [28], the L resolution is dominated by the spatial distribution of activated ${}^8\text{Li}$ isotopes inside the target and sleeve. The antineutrino creation point is distributed in the beam coordinate z according to an approximately uniform distribution, spanning the length of the 150 cm long sleeve. Although the spread in z dominates the smearing of the antineutrino baseline L , the distribution in terms of the transverse coordinates is taken into account as well.

The IsoDAR oscillation analysis follows the method of Ref. [31]. This analysis exploits the L/E dependence of oscillations, since L and E can be precisely reconstructed in the detector described. Eq. 1 is a good approximation for 3+1 (three active plus one sterile) disappearance fits to data, but in the case of 3+2 (three active plus two sterile), Eq. 1 is modified to accommodate Δm_{41}^2 , Δm_{51}^2 , and Δm_{45}^2 oscillations. If U is the mixing matrix, then the disappearance probabilities in the 3+1 and 3+2 scenarios are given by

$$P_{3+1} = 1 - 4|U_{e4}|^2(1 - |U_{e4}|^2)\sin^2(\Delta m_{41}^2 L/E) \quad (2)$$

$$\begin{aligned} P_{3+2} = 1 - 4[& (1 - |U_{e4}|^2 - |U_{e5}|^2) \times \\ & (|U_{e4}|^2 \sin^2(\Delta m_{41}^2 L/E) + \\ & |U_{e5}|^2 \sin^2(\Delta m_{51}^2 L/E)) + \\ & |U_{e4}|^2 |U_{e5}|^2 \sin^2(\Delta m_{45}^2 L/E)]. \end{aligned} \quad (3)$$

This assumes that contributions to disappearance from the μ and τ elements of the mixing matrix ($U_{\mu 4}$, $U_{\mu 5}$, $U_{\tau 4}$, and $U_{\tau 5}$) are negligible. We note that the current global fit improves significantly in the case of two sterile neutrinos [32].

Figure 3 illustrates the L/E -dependent signal for example 3+1 and 3+2 oscillation signals after five years of running. The observation of an oscillation wave, featuring multiple peaks and valleys for currently favored values of Δm^2 , makes this a highly compelling analysis. The wave also allows differentiation between 3+1 and 3+2 models in most oscillation scenarios. The 3+2 model-based oscillation probability shown in Fig. 3 utilizes the oscillation parameters given in Ref. [32]. These parameters represent the best fit of the world's appearance and disappearance data.

IsoDAR can quickly probe the oscillation parameter space indicative of one or more sterile neutrinos. As the antineutrino source described can be constructed within five years, we compare the IsoDAR 95% CL sensitivity to experiments that can be accomplished on this time scale. The global fit region, encompassing all appearance and disappearance measurements, is shown along with this comparison in Fig. 4. Note that the global fit [32] pulls the reactor anomaly allowed region significantly lower in Δm^2 due to the LSND and MiniBooNE appearance results, resulting in a $\Delta m^2 \sim 1\text{--}2$ eV 2 . As can be seen in Fig. 4, the statistics-limited IsoDAR sensitiv-

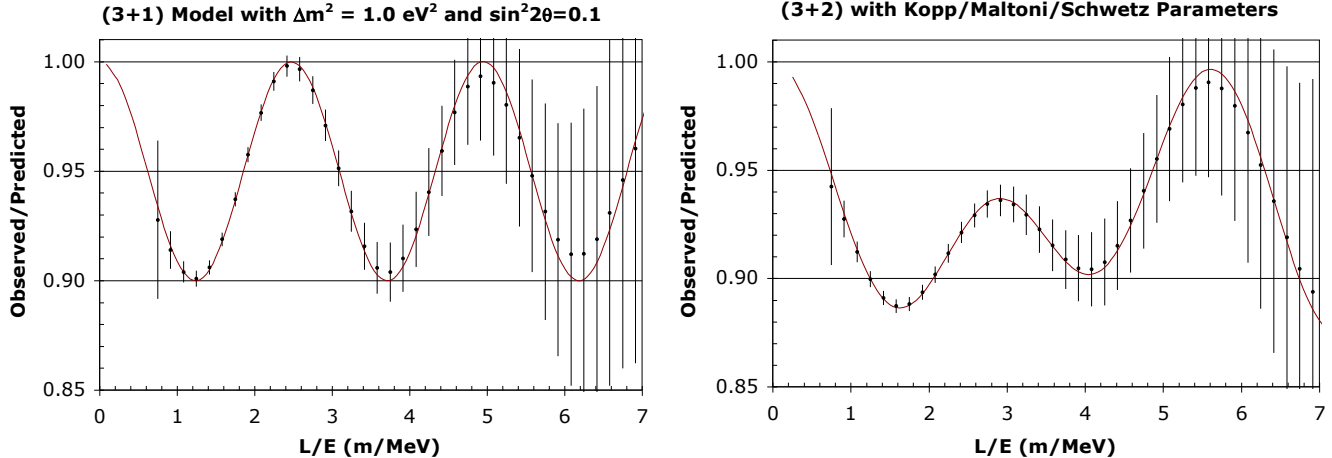


FIG. 3: The L/E dependence of two example oscillation signatures after five years of IsoDAR running. The solid curve is the oscillation probability with no smearing in the reconstructed position and energy. The 3+2 example (right) represents oscillations with the global best fit 3+2 parameters from Ref. [32].

ity covers the 3+1 allowed range [$\sin^2 2\theta = 0.067$ and $\Delta m^2 = 1 \text{ eV}^2$] at 20σ in five years of running. IsoDAR can rule out $\sin^2 2\theta = 0.067$, $\Delta m^2 = 1 \text{ eV}^2$ at 5σ in 4 months. The “shape-only” and “rate+shape” based sensitivities are shown in the plot. It is clear that the flux normalization uncertainty is only relevant for oscillation sensitivity at high Δm^2 ($\gtrsim 15 \text{ eV}^2$), a region where the rapid oscillation wave becomes difficult to resolve.

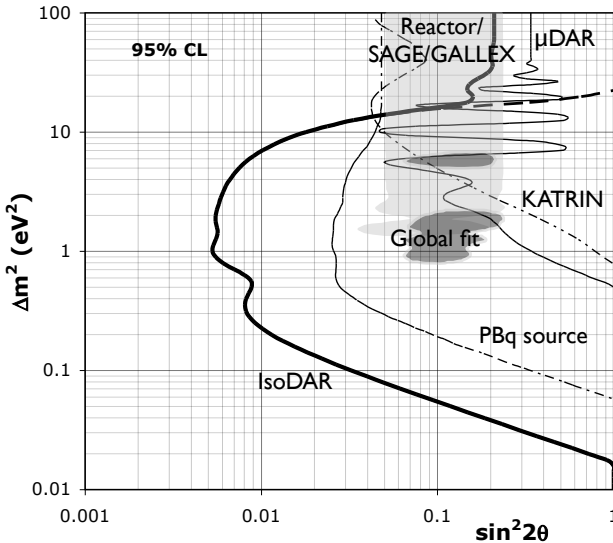


FIG. 4: The sensitivity of the IsoDAR experiment to electron antineutrino disappearance in a five year physics run. The sensitivities for both rate+shape (solid line) and shape-only (dashed line) are shown. The μ DAR [33] exclusion curve and Reactor+Gallium [3] allowed region are also shown, along with the expected sensitivities from the PBq source [34] and KATRIN [35] experiments.

The IsoDAR technique provides a high-intensity, low-energy source of antineutrinos with sensitivity to antineu-

trino oscillations near $\Delta m^2 \sim 1 \text{ eV}^2$. The experiment can perform compelling tests of models for new physics that explain high Δm^2 oscillations through the introduction of one or more sterile neutrinos. In a 3+1 model, IsoDAR can address the global fit region for electron flavor disappearance at 20σ (5σ) in five years (four months). In addition, the form of the oscillation wave can be reconstructed, allowing differentiation between the existence of 3+1 and 3+2 neutrinos. The large event sample also provides the possibility of a wide variety of other standard model tests, including a precise measurement of the weak mixing angle.

Acknowledgments

The authors thank the attendees of the Erice International School of Subnuclear Physics Workshop, Nov. 27-Dec. 5, 2011, for valuable discussions. Support for this

workshop was provided through the Majorana Centre from the INFN Eloisatron Project directed by Prof. Antonino Zichichi. JMC and MHS thank the National Science Foundation for support.

[1] A. Aguilar *et al.* [LSND Collaboration], Phys. Rev. D **64**, 112007 (2001).

[2] A.A. Aguilar-Arevalo *et al.* [MiniBooNE Collaboration], Phys. Rev. Lett. **105**, 181801 (2010).

[3] G. Mention, M. Fechner, T. Lasserre, T.A. Mueller, D. Lhuillier, M. Cribier and A. Letourneau, Phys. Rev. D **83**, 073006 (2011).

[4] C. Giunti and M. Laveder, Phys. Rev. C **83**, 065504 (2011).

[5] M. Sorel, J.M. Conrad and M.H. Shaevitz, Phys. Rev. D **70**, 073004 (2004).

[6] G. Karagiorgi, Z. Djurcic, J.M. Conrad, M.H. Shaevitz and M. Sorel, Phys. Rev. D **80**, 073001 (2009) [Erratum-ibid. D **81**, 039902 (2010)].

[7] C. Giunti and M. Laveder, Phys. Lett. B **706**, 200 (2011).

[8] K.N. Abazajian *et al.*, arXiv:1204.5379 [hep-ph] (2012).

[9] N.E. Davison, M.J. Canty, D.A. Dohan, and A. McDonald, Phys. Rev. C **10**, 50 (1974).

[10] Yu. S. Lutostansky and V.I. Lyashuk, Bull. Russ. Acad. Sci. **75**, 468 (2011).

[11] N.G. Basov and V.B. Rozanov, JETP Lett. **42**, 431 (1985).

[12] S. Abe *et al.* [KamLAND Collaboration], Phys. Rev. Lett. **100**, 221803 (2008).

[13] C. Kraus [SNO+ Collaboration], Prog. Part. Nucl. Phys. **57**, 150 (2006).

[14] A. Ianni [Borexino Collaboration], Nucl. Instrum. Meth. A **617**, 488 (2010).

[15] D. Campo, A. Calanna, L. Calabretta, D. Rifuggiato, M. Maggiore, L.A.C. Piazza, Proceedings of IPAC2011, San Sebastian, Spain, WEPS073 (2011).

[16] J.M. Conrad and M.H. Shaevitz, Phys. Rev. Lett. **104**, 141802 (2010).

[17] J. Alonso *et al.*, [DAEδALUS Collaboration] , arXiv:1006.0260 [physics.ins-det] (2010).

[18] <http://www.iba-cyclotron-solutions.com/products-cyclo/cyclone-70>

[19] http://www.bestcyclotron.com/product_70p.html

[20] R. Miracoli, L. Celona, G. Castro, D. Mascali, S. Gammino *et al.*, Rev. Sci. Instrum. **83**, 02A305 (2012).

[21] M. Reiser, *Theory and Design of Charged Particle Beams*, John Wiley & Sons, Inc. (1994).

[22] T. Mitsumoto, K. Fujita, T. Ogasawara, H. Tsutsui, S. Yajima, A. Maruhashi, Y. Sakurai, H. Tanaka, Proceedings of CYCLOTRONS 2010, Lanzhou, China, FRM2CC004 (2010).

[23] Y.J. Bi, A. Adelmann, R. Dölling, M. Humbel, W. Joho, M. Seidel, and T. Zhang, Phys. Rev. ST Accel. Beams **14**, 054402 (2011).

[24] P.F. Meads, IEEE Trans. Nucl. Sci. **30**, 2838 (1983).

[25] S. Agostinelli *et al.*, Nucl. Instr. & Meth. A **506**, 250 (2003).

[26] Evaluated Nuclear Data File ENDF/B-VII, www.nndc.bnl.gov/endf

[27] P. Vogel and J.F. Beacom, Phys. Rev. D **60**, 053003 (1999).

[28] A. Gando *et al.* [KamLAND Collaboration] Phys. Rev. D **83**, 052002 (2011).

[29] S. Abe *et al.* [KamLAND Collaboration], Phys. Rev. Lett. **100**, 221803 (2008).

[30] E. Guillian, arXiv:0809.1649 [hep-ph] (2008).

[31] S.K. Agarwalla, J.M. Conrad and M.H. Shaevitz, J. High Energy Phys. **12**, 085 (2011).

[32] J. Kopp, M. Maltoni and T. Schwetz, Phys. Rev. Lett. **107**, 091801 (2011).

[33] J.M. Conrad and M.H. Shaevitz, Phys. Rev. D **85**, 013017 (2012).

[34] M. Cribier *et al.*, Phys. Rev. Lett. **107**, 201801 (2011).

[35] J.A. Formaggio and J. Barrett, Phys. Lett. B **706**, 68 (2011).